INT. J. REMOTE SENSING, 2003, VOL. 24, NO. 4, 689–702

Taylor & Francis
Taylor & Francis Group

Noise estimation in remote sensing imagery using data masking

B. R. CORNER†, R. M. NARAYANAN*† and
S. E. REICHENBACH‡

† Department of Electrical Engineering, University of Nebraska, Lincoln, Nebraska 68588-0511, USA
‡ Department of Computer Science and Engineering, University of Nebraska, Lincoln, Nebraska 68588-0115, USA

(*Received 18 January 2001; in final form 13 November 2001*)

Abstract. Estimation of noise contained within a remote sensing image is essential in order to counter the effects of noise contamination. The application of convolution data-masking techniques can effectively portray the influence of noise. In this paper, we describe the performance of a developed noise-estimation technique using data masking in the presence of simulated additive and multiplicative noise. The estimation method employs Laplacian and gradient data masks, and takes advantage of the correlation properties typical of remote sensing imagery. The technique is applied to typical textural images that serve to demonstrate its effectiveness. The algorithm is tested using Landsat Thematic Mapper (TM) and Shuttle Imaging Radar (SIR-C) imagery. The algorithm compares favourably with existing noise-estimation techniques under low to moderate noise conditions.

1. Introduction

1.1. *Characteristics of noise*

Noise in remote sensing imagery degrades the interpretability of the data. Noise is produced by numerous factors including thermal effects, sensor saturation, quantization errors and transmission errors. Noise added to the data in an optical remote sensing system is typically independent of the data, and is generally additive in nature. This type of noise can generally be represented as a normally distributed (Gaussian), zero-mean random process with a probability density function (pdf) $f_x(x)$ given as

$$f_x(x)=\frac{1}{\sqrt{2\pi}\sigma_n}\,e^{-x^2/2\sigma_n^2} \tag{1}$$

where σ_n is the standard deviation of the noise process. The effect of an additive noise process, n_a, on an image digital number (DN), at the ith and jth pixel can then be modelled as the summation of the true signal, S, with the noise as shown by

$$\mathrm{DN}(i,j)=S(i,j)+n_a(i,j) \tag{2}$$

*Corresponding author: e-mail: rnarayanan@unl.edu

International Journal of Remote Sensing
ISSN 0143-1161 print/ISSN 1366-5901 online © 2003 Taylor & Francis Ltd
http://www.tandf.co.uk/journals
DOI: 10.1080/01431160210164271

Radar remote sensing systems, such as a Synthetic Aperture Radar (SAR), are affected by multiplicative noise in addition to additive noise. Multiplicative (speckle) noise is produced by the coherent superposition of spatially random multiple scattering sources within the resolution volume of the radar. The scattered waves constructively or destructively interfere with each other causing a speckled appearance to the image. This type of noise can be expressed as a unity-mean normal random process with pdf given by

$$f_x(x)=\frac{1}{\sqrt{2\pi}\sigma_{\mathrm{n}}}\,\mathrm{e}^{-(x-1)^2/2\sigma_{\mathrm{n}}^2} \tag{3}$$

The effect of multiplicative noise, n_{m}, on the image can be modelled as

$$\mathrm{DN}(i,j)=S(i,j)n_{\mathrm{m}}(i,j) \tag{4}$$

This type of noise is dependent on the reflected signal magnitude.

1.2. *Data masking technique*

It is often desired to estimate the noise standard deviation of imagery so that the image may be suitably filtered to remove the noise. Numerous techniques have been developed to filter and estimate the standard deviation of noise (Bracho and Sanderson 1985, Voorhees and Poggio 1987, Lee and Hoppel 1989, Meer *et al.* 1990, Olsen 1993, Rank *et al.* 1999). Spatial filtering of the image can be performed by convolving the image with a small moving window (mask) which implements a desired frequency characteristic. Each pixel of the original image is replaced by a weighted average of the product of the window and the neighbouring pixels. This process is typically referred to as discrete convolution filtering or data masking (Gonzalez and Woods 1992). If a 3×3 mask template is given by

$$\begin{matrix} z_1 & z_2 & z_3 \\ z_4 & z_5 & z_6 \\ z_7 & z_8 & z_9 \end{matrix} \tag{5}$$

the new pixel values of the image are

$$\mathrm{DN}_{\mathrm{new}}=\sum_{i=1}^{9} z_i \mathrm{DN}_{i_{\mathrm{orig}}} \tag{6}$$

where the DNs represent the brightness values of the pixels. The data mask is moved one pixel at a time with the pixel being filtered directly in the centre of the mask, and the neighbouring pixels have equation (6) applied sequentially until every pixel has been filtered.

One method to estimate the noise standard deviation is to first filter the image to remove the image structure, thereby leaving only the noise. It has been shown that a Laplacian mask can be useful for image structure suppression (Immerkaer 1996). The Laplacian of a function, $f(x, y)$, is given by

$$\nabla^2 f=\partial^2 f/\partial x^2+\partial^2 f/\partial y^2 \tag{7}$$

which can be written in discrete form as (Rosenfeld and Kak 1982)

$$\nabla^2 f\equiv f(x+1, y)+f(x-1, y)+f(x, y+1)+f(x, y-1)-4f(x, y) \tag{8}$$

The second-order nature of the Laplacian tends to make it sensitive to noise, while suppressing smoothly varying and uniform regions and enhancing edges. The

difference of two Laplacians can be used as well for image suppression. One variation of a 3×3 data mask associated with the difference of two Laplacians can be written as

$$\begin{matrix} 1 & -2 & 1 \\ -2 & 4 & -2 \\ 1 & -2 & 1 \end{matrix} \tag{9}$$

Using the difference of two Laplacians further increases the sensitivity of the mask to noise. In remote sensing imagery, there generally exist a high degree of correlation between a pixel and the surrounding neighbourhood. Laplacian masking essentially takes the difference of the difference of adjacent pixels in an image. Because of the correlatedness of the image, the Laplacian image suppresses a majority of the original image structure, leaving mostly noise remaining.

Because some edge structure information remains after applying the Laplacian mask shown in equation (9), it is desirable to further filter the image to remove the edges. First, it is necessary to detect the edges before they can be removed. The gradient of a function, $f(x, y)$, is

$$\nabla f = \begin{bmatrix} \partial f/\partial z \\ \partial f/\partial y \end{bmatrix} \tag{10}$$

which gives the maximum rate of change of f at (x, y). The magnitude of this vector provides a basis for a data mask in which the edges can be detected. An approximation to the magnitude of equation (10), using the notation of equation (5), can be given as (Jensen 1996)

$$|\nabla f| \approx |(z_3 + 2z_6 + z_9) - (z_1 + 2z_4 + z_7)| + |(z_1 + 2z_2 + z_3) - (z_7 + 2z_8 + z_9)| \tag{11}$$

which results in the masks

$$f_x = \begin{matrix} -1 & 0 & 1 \\ -2 & 0 & 2, \\ -1 & 0 & 1 \end{matrix} \qquad f_y = \begin{matrix} 1 & 2 & 1 \\ 0 & 0 & 0 \\ -1 & -2 & -1 \end{matrix} \tag{12}$$

The masks in equation (12) can be simultaneously applied to an image to form the magnitude operation

$$|\nabla f| = \sqrt{f_x^2 + f_y^2} \tag{13}$$

This is commonly referred to as a Sobel edge detector (Jensen 1996). By thresholding the resulting edge-detected image with a specified value, a binary edge map can be obtained. An outline of the developed noise standard deviation estimation procedure can be seen from the flowchart in figure 1.

1.3. *Image selection and description*

To investigate the above technique for noise standard deviation estimation in remote sensing images, various datasets were considered. These included simulated textures, Landsat Thematic Mapper (TM) data, and Shuttle Imaging Radar (SIR-C) data. In figure 2, the selected textural images are shown. All the textures have pixel dimensions of 256×256. The horizontal striped image contains alternating, four-pixel wide, uniform pixels of DN values 64 and 192, respectively. This type of texture graphically represents agricultural row-crops or orchards. The chequerboard image

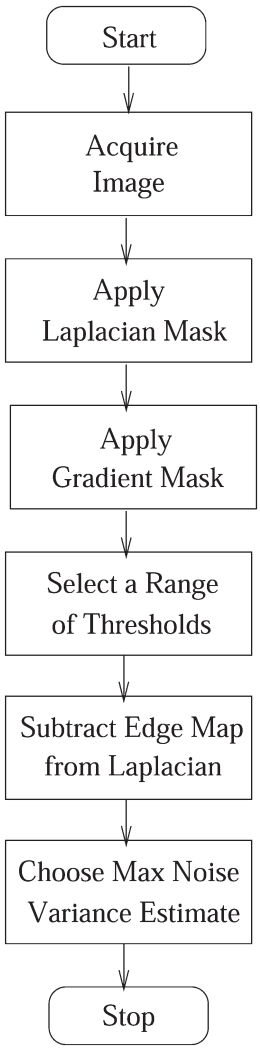

Figure 1. Outline of the noise-estimation procedure.

contains alternating 8×8 blocks, again with pixel DN values of 64 and 192. This is representative of a series of well laid out agricultural plots. For the random block image, blocks of pixels ranging in size from 4×4 to 20×20 with DN values 64 and 192 were randomly placed throughout a uniform background of pixel DN value 127 at an approximate 30% density. This situation represents a case where small scattered plots of vegetation of different sizes exist in an otherwise homogeneous background. The uniform image is a pure grey image with all pixel DN values set to 127.

For noise estimation from Landsat TM imagery, the three images shown in figure 3 were selected. The wavelengths and corresponding spectral locations for the TM sensors are given in table 1. TM Images 1 and 2 are TM bands 7 and 3, respectively. The scene shown is along the Missouri River near the convergence of the Nebraska, Iowa and Missouri state borders. Agricultural uses are the predominant land cover of the scene. TM Image 3 is a TM band 7 image centred on the

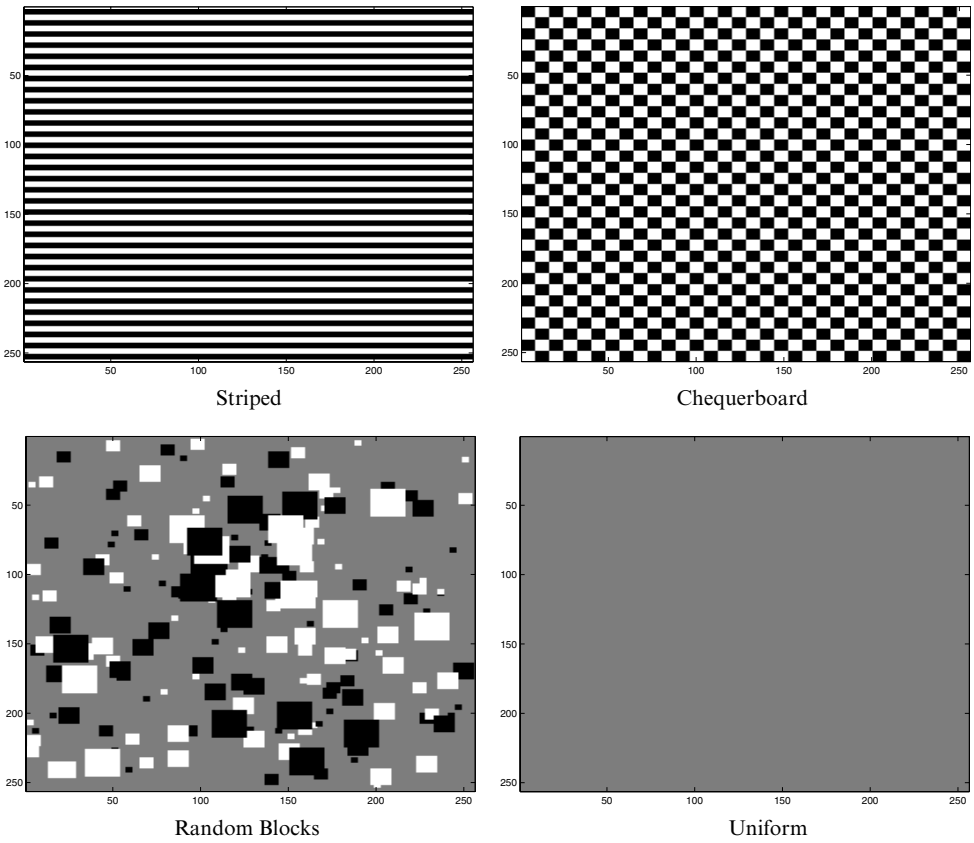

Figure 2. Textural images used for noise estimation.

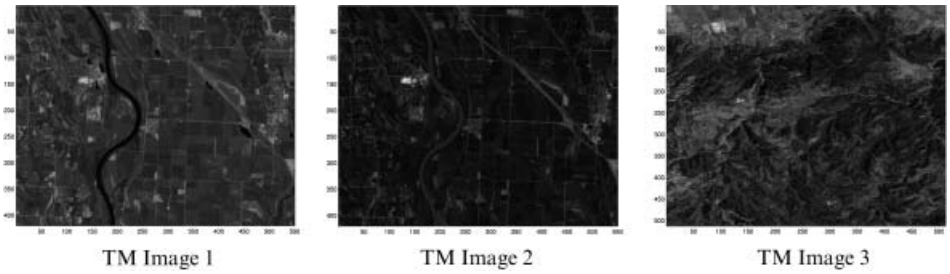

Figure 3. TM images used for noise estimation.

Table 1. Landsat TM sensor wavelengths and spectral locations.

Band no.	Wavelength (μm)	Spectral location
1	0.45–0.52	Blue–green
2	0.52–0.60	Green
3	0.63–0.69	Red
4	0.76–0.90	Near IR
5	1.55–1.75	Mid IR
6	10.4–12.5	Thermal IR
7	2.08–2.35	Mid IR

Black Hills region of South Dakota. The terrain here is much more rugged and generally forested.

Two type of SIR-C data were also selected for noise estimation as shown in figure 4. The radar wavelengths and polarizations for the SIR-C are shown in table 2. The SIR-C images used correspond to L-band and HH polarization amplitude data. The images show a subset of both single-look complex (SLC) and multiple-look complex (MLC) amplitude data taken from an agricultural region in the Upper Peninsula of Michigan. The SIR-C MLC image was generated from the full SLC image by using 10 multilooks in azimuth and two in the range direction. Both images are 256×256 in size and can be seen to contain inherent multiplicative noise.

2. Noise simulation results

2.1. *Additive noise*

To estimate the noise standard deviation of a single image, a data-masking approach was devised. Following the model of equation (2), normally distributed, uncorrelated, zero-mean additive noise was generated for several different standard deviation values. The noise was then added to the textural, TM and SIR-C images to simulate a noisy image. Any inherent noise in the original TM and SIR-C data was considered to be part of the data. After applying the noise, the pixel DN values were rounded to the nearest integer.

An example of the procedure using TM Image 1 is described below. The estimation procedure begins by first applying the Laplacian mask of equation (9) to the image. An example of the resulting masked image is shown in figure 5 for TM Image 1. The image in figure 5 contains mostly noise but not all the edge structure was suppressed. Portions of the river and a road bisecting the eastern portion of the image are the most prominent remaining features. The presence of the edges in the Laplacian masked image increases the non-noise variance of the image, which is

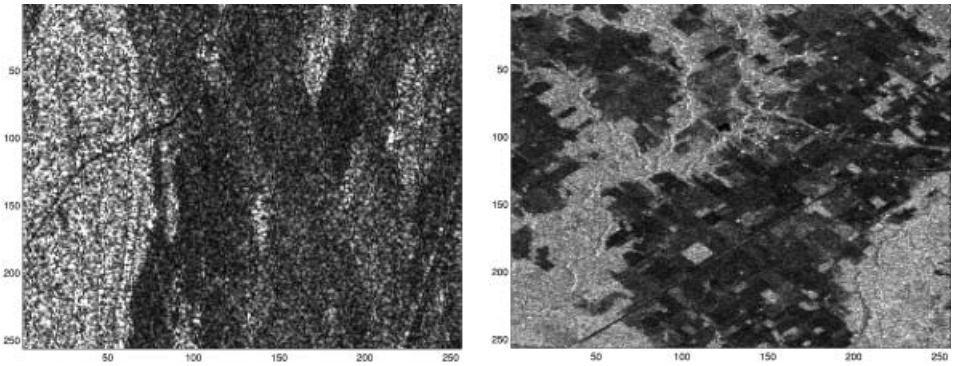

Figure 4. SIR-C images used for noise estimation.

Table 2. SIR-C wavelengths and polarizations.

Band	Wavelength (cm)	Polarization
L	23.5	HH, HV, VV, VH
C	5.8	HH, HV, VV, VH

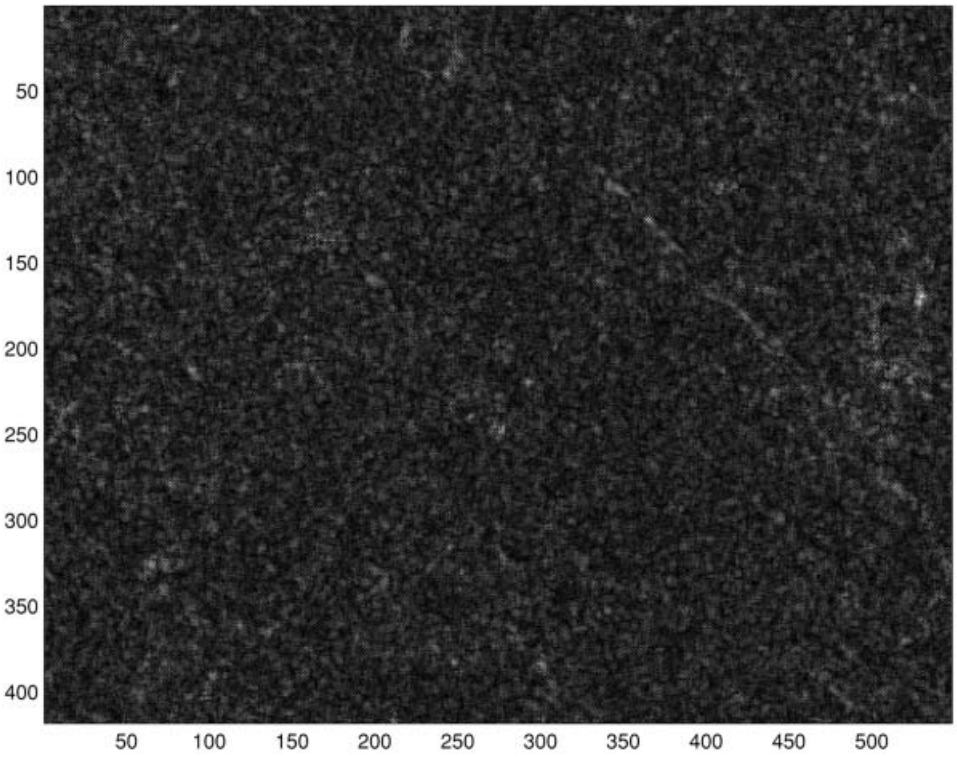

Figure 5. Result of applying a Laplacian mask to TM Image 1 with a noise variance of 10.0.

undesirable. To reduce the variance contribution of the edges, an edge map was required. The Sobel edge-detection masks of equation (12) were applied to the Laplacian filtered image to determine the edge locations. A user-specified threshold was then required to form an edge/no-edge binary decision map from the Sobel filtered image. Pixel values above this threshold were determined to be edges while those below were noise. The corresponding edge map for TM Image 1 is shown in figure 6, in which the boundaries of the road and river edges are clearly seen. Using the edge map, the corresponding pixels were removed from the Laplacian image to reduce the edge variance contribution. The optimal threshold was established by specifying a range of thresholds and choosing the one in which the resulting variance of the Laplacian image, with the corresponding edge map subtracted from it, was a maximum. A plot of the resulting estimated noise variance as a function of the selected threshold value is shown in figure 7, from which the optimum threshold was deduced to be 3.5. Thresholding plots for the other TM and SIR-C images generally followed a similar type of curve. The threshold corresponding to the maximum variance was chosen for the final estimation.

The final step in the noise standard deviation estimation process involves finding the local standard deviations of the edge-removed image. The standard deviation of 9×9 blocks of pixels from the edge-removed Laplacian image were calculated, and a histogram of the results plotted. Pixels that were mapped as edges are ignored in calculating the local standard deviations. This results in some local standard deviations being determined from less than the maximum available set of pixels. The

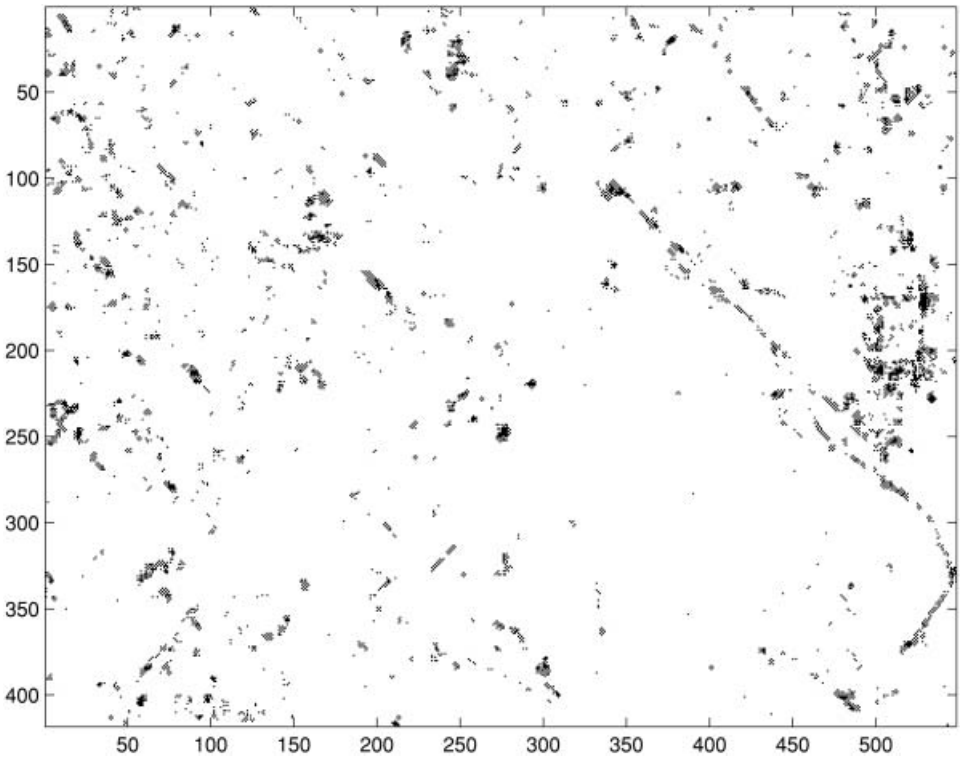

Figure 6. Edge map from TM Image 1 with a noise variation of 10.0 and a threshold of 3.5.

histogram of the local standard deviations from TM Image 1, with an added noise variance of 10.0, is shown in figure 8. Some of the original image structure and edge information remains even after the filtering and edge removal. By using a histogram of the standard deviation of small blocks from the image, one can make the final estimation of the noise standard deviation. Through experimentation, it was discovered that the median value of the histogram supplied the most accurate final estimate.

The estimated noise standard deviations, $\hat{\sigma}_n$, and the error (difference) between the actual and estimated value, $\bar{\varepsilon}$, for several different standard deviations of additive noise, applied to the textural, TM and SIR-C images, are shown in tables 3–5. The tables show the average of 20 iterations for each noise standard deviation run. The results show that the estimation technique performs quite well in most cases.

In the TM imagery, the ruggedness of the landcover in TM Image 3 resulted in a noiseless standard deviation of 16.022, as opposed to 8.803 for TM Image 1, and 5.732 for TM Image 2. Some of this additional initial image structure standard deviation remains in the the final image used for the noise estimation, and generally results in a larger mean error for the estimates. This is particularly the case for small added noise variances. The textural images contain lower image variance compared to the TM and SIR-C images, and the error of the noise estimates are correspondingly lower.

The SIR-C imagery resulted in the highest noise standard deviation errors. Because of the inherent multiplicative noise in the imagery, the initial standard deviations of the images are 60.48 and 46.62 for the SLC and MLC images,

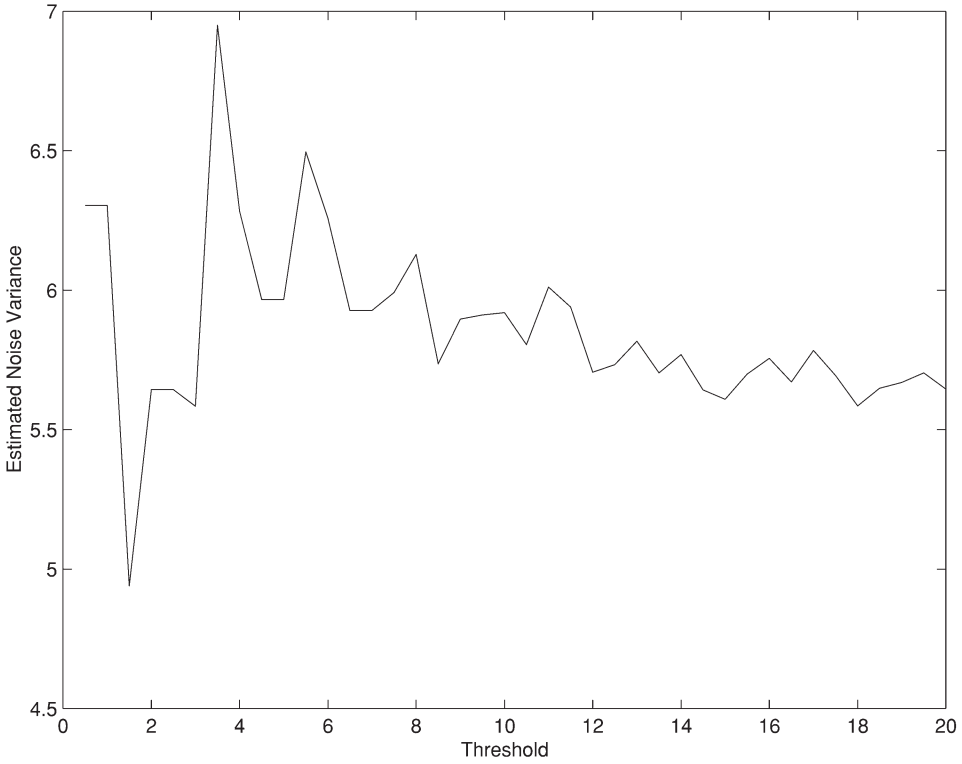

Figure 7. Estimated noise variances over a range of thresholds from TM Image 1 with a noise variance of 10.0. The chosen optimal threshold was 3.5, which maximizes the estimated noise variance.

respectively. The multiplicative noise tends to dominate the images and renders the additive noise estimates unreliable. Statistical parameters of the image are altered by the summation of the inherent and applied additive noise random variables. The SIR-C MLC estimates are slightly improved from the SLC case due to the smoothing effect caused by the integration of the full SLC image. The noise-estimation procedure does not appear to be effective in extracting additive noise estimates in the presence of multiplicative noise.

For the uniform image, it was found that changing the intensity of the pixel DN value from 127 to any other value did not change the noise standard deviation estimate. This suggests that the estimation method is independent of variations in homogeneous intensity.

2.2. *Multiplicative noise*

To simulate multiplicative noise, the model of equation (4) was applied to the images of figures 2–4. After including the multiplicative noise, the pixel DN values were rounded to the nearest integer, and the logarithms of the DN values were computed. This transforms the multiplicative noise into an additive noise in the logarithm domain. The noise estimation procedure described previously was then applied to the resulting image. For the final estimate in this case, however, the variance of histogram was subtracted from the median value of the histogram. The

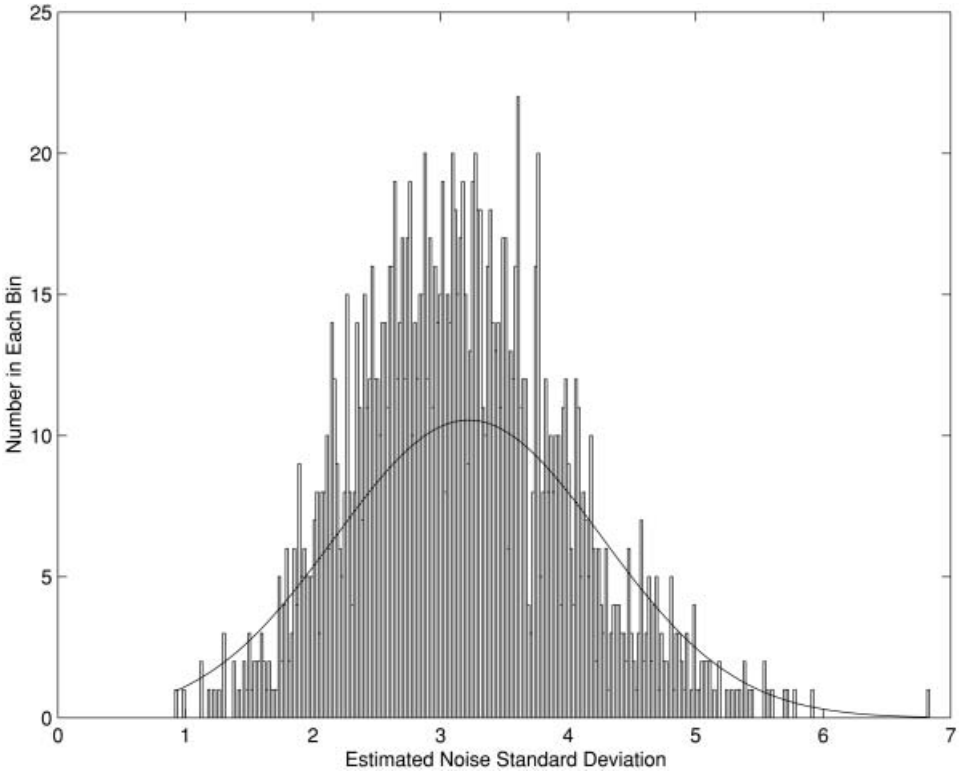

Figure 8. Histogram of the local standard deviations of 9×9 blocks from TM Image 1 with a noise variance of 10.0. An optimal Gaussian fit to the histogram is shown for reference.

Table 3. Additive noise estimation results for simulated textural imagery.

Noise parameter		Striped		Chequerboard		Random blocks		Uniform	
σ_n^2	σ_n	$\hat{\sigma}_n$	$\bar{\varepsilon}$	$\hat{\sigma}_n$	$\bar{\varepsilon}$	$\hat{\sigma}_n$	$\bar{\varepsilon}$	$\hat{\sigma}_n$	$\bar{\varepsilon}$
10.000	3.162	2.618	0.544	2.689	0.465	2.618	0.544	2.510	0.652
5.000	2.236	2.216	0.020	1.883	0.353	2.168	0.068	2.092	0.144
3.000	1.732	1.601	0.131	1.820	−0.088	1.595	0.137	1.573	0.159
2.000	1.414	1.241	0.173	1.314	0.100	1.225	0.189	1.358	0.056
1.000	1.000	0.939	0.061	0.977	0.023	0.943	0.057	0.957	0.043
0.500	0.707	0.701	0.006	0.709	−0.002	0.686	0.021	0.704	0.003

logarithm introduces a compression of the dynamic range of the pixel DN values, and it was discovered through experimentation that subtracting the variance provided the best estimate. The estimation results for the textural, TM and SIR-C images can be seen in tables 6–8. The results show that the method performs well for the range of multiplicative noises. The highest values of multiplicative noise contain the largest estimation error. This is a direct result of the window size in determining the local noise standard deviations, and is discussed in greater detail in §2.3. Increasing the block size greater than 9×9 in the histogram analysis will reduce the overall estimation error for high noise values at a cost of increasing the estimation

Table 4. Additive noise estimation results for TM imagery.

Noise parameter		TM Image 1		TM Image 2		TM Image 3	
σ_n^2	σ_n	$\hat{\sigma}_{n1}$	$\bar{\varepsilon}_1$	$\hat{\sigma}_{n2}$	$\bar{\varepsilon}_2$	$\hat{\sigma}_{n3}$	$\bar{\varepsilon}_3$
10.000	3.162	2.636	0.526	2.517	0.637	2.772	0.390
5.000	2.236	1.938	0.298	1.888	0.348	2.213	0.023
3.000	1.732	1.844	−0.112	1.544	0.188	1.661	0.071
2.000	1.414	1.403	0.011	1.321	0.093	1.601	−0.187
1.000	1.000	1.065	−0.065	1.008	−0.008	1.405	−0.405
0.500	0.707	0.837	−0.130	0.803	−0.096	1.257	−0.550

Table 5. Additive noise estimation results for SIR-C imagery.

Noise parameter		SIR-C SLC		SIR-C MLC	
σ_n^2	σ_n	$\hat{\sigma}_{n1}$	$\bar{\varepsilon}_1$	$\hat{\sigma}_{n2}$	$\bar{\varepsilon}_2$
10.000	3.162	4.354	−1.192	1.423	1.739
5.000	2.236	0.422	1.814	0.421	1.815
3.000	1.732	0.233	1.499	1.192	0.540
2.000	1.414	0.215	1.199	0.643	0.771
1.000	1.000	1.502	−0.502	1.377	−0.377
0.500	0.707	0.076	0.631	0.863	−0.156

Table 6. Multiplicative noise estimation results for simulated textural imagery.

Noise parameter		Striped		Chequerboard		Random blocks		Uniform	
σ_n^2	σ_n	$\hat{\sigma}_{n1}$	$\bar{\varepsilon}_1$	$\hat{\sigma}_{n2}$	$\bar{\varepsilon}_2$	$\hat{\sigma}_{n3}$	$\bar{\varepsilon}_3$	$\hat{\sigma}_{n4}$	$\bar{\varepsilon}_4$
0.0001	0.0100	0.0097	0.0003	0.0098	0.0002	0.0094	0.0006	0.0105	−0.0005
0.0010	0.0316	0.0294	0.0022	0.0295	0.0021	0.0295	0.0021	0.0293	0.0023
0.0050	0.0707	0.0657	0.0050	0.0660	0.0047	0.0661	0.0046	0.0657	0.0050
0.0100	0.1000	0.0932	0.0068	0.0972	0.0028	0.0935	0.0065	0.0933	0.0067
0.1000	0.3162	0.2107	0.1055	0.2227	0.0935	0.1913	0.1249	0.1916	0.1246

Table 7. Multiplicative noise estimation results for TM imagery.

Noise parameter		TM Image 1		TM Image 2		TM Image 3	
σ_n^2	σ_n	$\hat{\sigma}_{n1}$	$\bar{\varepsilon}_1$	$\hat{\sigma}_{n2}$	$\bar{\varepsilon}_2$	$\hat{\sigma}_{n3}$	$\bar{\varepsilon}_3$
0.0001	0.0100	0.0209	−0.0109	0.0216	−0.0116	0.0495	−0.0395
0.0010	0.0316	0.0396	−0.0080	0.0387	−0.0071	0.0592	−0.0276
0.0050	0.0707	0.0718	−0.0011	0.0706	0.0001	0.0857	−0.0150
0.0100	0.1000	0.0962	0.0038	0.0968	0.0032	0.1091	−0.0091
0.1000	0.3162	0.1487	0.1675	0.1697	0.1465	0.1780	0.1382

error of the lower noise values. For all the textural images, the estimation errors are very similar. Although a direct comparison with the additive case is not possible, the multiplicative results display similar tendencies.

For the SIR-C imagery, the procedure was first used to estimate the inherent

Table 8. Multiplicative noise estimation results for SIR-C imagery.

Noise parameter		SIR-C SLC		SIR-C MLC	
σ_n^2	σ_n	$\hat{\sigma}_{n1}$	$\bar{\varepsilon}_1$	$\hat{\sigma}_{n2}$	$\bar{\varepsilon}_2$
0.0001	0.0100	0.339	−0.329	0.160	−0.150
0.0010	0.0316	0.341	−0.309	0.164	−0.132
0.0050	0.0707	0.350	−0.279	0.172	−0.101
0.0100	0.1000	0.350	0.250	0.182	0.082
0.1000	0.3162	0.219	0.097	0.173	0.143

noise standard deviation without applying any additional simulated noise. The inherent multiplicative noise standard deviation was computed as 0.321 for SLC and 0.159 for MLC cases. The noise estimates after applying simulated noise increase from the inherent value with increasing applied noise, although it is observed that the inherent multiplicative noise contribution is still dominant. The inherent multiplicative noise standard deviations are similar to Lee (1986). Some effects of the windowing begin to occur at $\sigma_n^2 = 0.0100$. The results seem to indicate that the algorithm can sufficiently estimate the inherent speckle noise of a radar image. The estimates, after applying simulated noise, tend to be biased due to the change in the pdf of the image by the multiplication of the inherent and applied noise random variables.

2.3. *Effect of histogram window size*

For small values of additive noise, the differences between any residual image structure information and the noise become less defined and tend to result in higher estimation errors. This is particularly the case with the TM imagery. For all the images, higher absolute estimation errors also occurred for the largest added noise values. This was observed to be related to the block size used in producing the histogram in the previously described estimation procedure. Taking the standard deviation of block sizes larger than 9×9 in the histogram is required to improve the estimate for the largest noise values due to the increased variability of the individual pixels caused by the noise. Use of a larger subset of the image when calculating the local standard deviations of the noise, increases the number of sample points and results in a better representation of the standard deviation. The trade-off is that, while the higher noise estimates are improved, the lower noise estimates are more error-prone. This occurs since the probability of having pixels with a greater variance from the mean value (outliers) increases by using a larger subset. This can be directly seen in tables 9 and 10 using three different window sizes on the uniform textural image in figure 2, and TM Image 1 in figure 3. For the TM image, the estimation error for small noise values is much larger for larger window sizes than for the uniform image which contains an initial noise-free variance of zero.

Modifications to the estimation algorithm to dynamically choose a histogram window size based on an intermediate noise estimate are currently being explored.

2.4. *Comparison with existing methods*

The performance of the estimation method developed in this paper was compared with existing published techniques. In table 11, estimations using these methods are shown for two methods for the additive noise case. The uniform images in figure 2

Table 9. Additive noise estimation results as a function of histogram window size for the uniform textural case.

Noise parameter		9×9 Window		15×15 Window		25×25 Window	
σ_n^2	σ_n	$\hat{\sigma}_n$	$\bar{\varepsilon}$	$\hat{\sigma}_n$	$\bar{\varepsilon}$	$\hat{\sigma}_n$	$\bar{\varepsilon}$
10.000	3.162	2.510	0.652	2.827	0.335	2.994	0.168
5.000	2.236	2.092	0.144	2.167	0.069	2.280	−0.044
3.000	1.732	1.573	0.159	1.648	0.084	1.730	0.002
2.000	1.414	1.358	0.056	1.348	0.066	1.413	0.001
1.000	1.000	0.957	0.043	1.013	−0.013	1.027	−0.027
0.500	0.707	0.704	0.003	0.737	−0.030	0.753	−0.046

Table 10. Additive noise estimation results as a function of histogram window size for TM Image 1.

Noise parameter		9×9 Window		15×15 Window		25×25 Window	
σ_n^2	σ_n	$\hat{\sigma}_n$	$\bar{\varepsilon}$	$\hat{\sigma}_n$	$\bar{\varepsilon}$	$\hat{\sigma}_n$	$\bar{\varepsilon}$
10.000	3.162	2.636	0.526	3.186	−0.024	3.140	0.022
5.000	2.236	1.938	0.298	2.275	−0.039	2.272	−0.036
3.000	1.732	1.844	−0.112	1.789	−0.057	1.839	−0.107
2.000	1.414	1.403	0.011	1.422	−0.008	1.469	−0.055
1.000	1.000	1.065	−0.065	1.179	−0.179	1.201	−0.201
0.500	0.707	0.837	−0.130	0.916	−0.209	0.933	−0.226

Table 11. Comparative additive noise estimation results.

Noise parameter		TM Image 1			TM Image 2			TM Image 3			Uniform		
σ_n^2	σ_n	$\bar{\varepsilon}_{avg}$	$\bar{\varepsilon}_{FNV}$	$\bar{\varepsilon}$	$\bar{\varepsilon}_{avg}$	$\bar{\varepsilon}_{FNV}$	$\bar{\varepsilon}$	$\bar{\varepsilon}_{avg}$	$\bar{\varepsilon}_{FNV}$	$\bar{\varepsilon}$	$\bar{\varepsilon}_{avg}$	$\bar{\varepsilon}_{FNV}$	$\bar{\varepsilon}$
3.000	1.732	0.896	0.231	0.112	0.485	0.138	0.188	2.395	0.882	0.071	0.077	0.015	0.159
2.000	1.414	1.039	0.278	0.011	0.594	0.169	0.093	2.605	1.000	0.187	0.053	0.021	0.056
1.000	1.000	1/263	0.368	0.065	0.773	0.240	0.008	2.907	1.199	0.405	0.019	0.034	0.043
0.500	0.707	1.456	0.468	0.130	0.937	0.306	0.096	3.143	1.376	0.550	0.014	0.054	0.003

and the TM images in figure 3 were used for the analysis. Simulated normally distributed additive noise was applied to the images, and the resulting pixel DN values were rounded to the nearest integer. The mean noise standard deviation of 20 separate estimates for each noise level is shown. The first comparative method is a moving average using a 9×9 window. This method is widely used due to the ease with which it can be implemented. The second is the method developed by Immerkaer (1996). In this method, a Laplacian mask is used to provide a fast method for additive noise estimation. In table 11, $\bar{\varepsilon}_{avg}$ and $\bar{\varepsilon}_{FNV}$ refer to the errors in noise standard deviation for the moving average and the Immerkaer models, respectively, while $\bar{\varepsilon}$ refers to our method. Our described method compares favourably with the other methods for all of the displayed relatively low noise levels. Without any adjustments to the window size used to calculate the local noise standard deviations, the performance of the method tends to decline with a higher amount of noise.

For noise variances greater than approximately 3.0, our described method tends to underperform existing techniques. It is suggested that the described method be used primarily for low to moderate amounts of noise. Adjusting the window size to span a larger sample space is necessary to achieve accurate estimations of larger noise standard deviations. If some *a priori* rough estimate of the amount of noise present in an image is available, it could be used as a basis for a decision rule in determining the appropriate window size. The final noise estimate itself could also be used in an iterative procedure to adjust the window size to produce an improved estimate if no *a priori* information is available. These topics are currently being explored.

3. Conclusions and future work

A technique has been developed in which Laplacian and gradient data masks are used to estimate the additive and multiplicative noise standard deviations in an image. The estimation was shown to perform best for low to moderate levels of both additive and multiplicative noise applied to the imagery. Increasing the window size to calculate the local standard deviations for the histogram tends to improve the estimates for higher amounts of noise. Comparisons of the estimation method with currently existing noise-estimation techniques show favourable results. Further quantification of the relationship between the window size of the local standard deviation used in the histogram analysis and the initial image variance on the resulting noise estimates are being explored.

Acknowledgements

The authors thank the NASA EPSCoR programme for their support of this research through the Nebraska Space Grant Consortium.

References

Bracho, R., and Sanderson, A. C., 1985, Segmentation of images based on intensity gradient information. *Proceedings of IEEE Computer Society Conference on Computer Vision and Pattern Recognition, June 1985* (San Francisco: IEEE), pp. 341–347.

Gonzalez, R. C., and Woods, R. E., 1992, *Digital Image Processing* (Reading, Massachusetts: Addison-Wesley).

Immerkaer, J., 1996, Fast noise variance estimation. *Computer Vision and Image Understanding*, **64**, 300–302.

Jensen, J. R., 1996, *Introductory Digital Image Processing: A Remote Sensing Perspective*, 2nd edn (Englewood Cliffs, New Jersey: Prentice Hall).

Lee, J. S., 1986, Speckle suppression and analysis for synthetic aperture radar images. *Optical Engineering*, **25**, 636–643.

Lee, J. S., and Hoppel, K., 1989, Noise-modelling and estimation of remotely-sensed images. *Proceedings of the International Geoscience and Remote Sensing Symposium, July 1989* (Vancouver: IEEE), vol. 2, pp. 1005–1008.

Meer, P., Jolion, J.-M., and Rosenfeld, A., 1990, A fast parallel algorithm for blind estimation of noise variance. *IEEE Transactions on Pattern Analysis and Machine Intelligence*, **12**, 216–223.

Olsen, S. I., 1993, Estimation of noise in images: an evaluation. *CVGIP: Graphical Models and Image Processing*, **55**, 319–323.

Rank, K., Lendi, M., and Unbehauen, R., 1999, Estimation of image noise variance. *Proceedings on Vision, Image and Signal Processing*, **146**, 80–84.

Rosenfeld, A., and Kak, A. C., 1982, *Digital Image Processing*, vol. 2 (New York: Academic Press).

Voorhees, H., and Poggio, T., 1987, Detecting blobs as textons in natural images. *Proceedings of the Image Understanding Workshop, February 1987* (Los Angeles: DARPA), pp. 892–899.